Geophysical Research Letters

RESEARCH LETTER
10.1029/2024GL110633

The Sensitivity of the Spatial Pattern of Sea Level Changes to the Depth of Antarctic Meltwater Fluxes

Ian Eisenman[1], **Aurora Basinski-Ferris**[2], **Emma Beer**[3], **and Laure Zanna**[2]

[1]Scripps Institution of Oceanography, University of California San Diego, La Jolla, CA, USA, [2]Courant Institute of Mathematical Sciences, New York University, New York, NY, USA, [3]Department of Earth, Environmental and Planetary Sciences, Rice University, Houston, TX, USA

Key Points:

- The depth at which Antarctic meltwater enters the ocean influences global sea level change patterns simulated with an idealized model
- The sea level change patterns tend to travel more slowly across the global ocean when meltwater fluxes occur at depth
- The propagation speed of the pattern is dictated primarily by the steric response to the depth of the meltwater fluxes

Supporting Information:

Supporting Information may be found in the online version of this article.

Correspondence to:

I. Eisenman,
eisenman@ucsd.edu

Citation:

Eisenman, I., Basinski-Ferris, A., Beer, E., & Zanna, L. (2024). The sensitivity of the spatial pattern of sea level changes to the depth of Antarctic meltwater fluxes. *Geophysical Research Letters*, *51*, e2024GL110633. https://doi.org/10.1029/2024GL110633

Received 6 JUN 2024
Accepted 11 SEP 2024

Abstract Regional patterns of sea level rise are affected by a range of factors including glacial melting, which has occurred in recent decades and is projected to increase in the future, perhaps dramatically. Previous modeling studies have typically included fluxes from melting glacial ice only as a surface forcing of the ocean or as an offline addition to the sea surface height fields produced by climate models. However, observational estimates suggest that the majority of the meltwater from the Antarctic Ice Sheet actually enters the ocean at depth through ice shelf basal melt. Here we use simulations with an ocean general circulation model in an idealized configuration. The results show that the simulated global sea level change pattern is sensitive to the depth at which Antarctic meltwater enters the ocean. Further analysis suggests that the response is dictated primarily by the steric response to the depth of the meltwater flux.

Plain Language Summary The time-varying pattern of sea level rise is projected to cause some coastal communities to be impacted more than others during the coming century. This pattern is influenced by the melting of Antarctic ice. Previous modeling studies have typically injected this meltwater at the ocean surface, despite observational evidence suggesting that it enters the ocean primarily at depth. Here we use simulations with a model in an idealized configuration to investigate how the sea level change pattern depends on the depth at which Antarctic meltwater enters the ocean. We find that the sea level change signal tends to travel more slowly across the global ocean when the meltwater enters the ocean at depth. These results have implications for projected regional sea level changes in response to the melting of Antarctic ice.

1. Introduction

Sea level rise is expected to be a major consequence of global warming, with costs from coastal flooding estimated to reach 3% of global GDP by 2100 (Jevrejeva et al., 2018). This impact depends crucially on the time-varying spatial pattern of future sea level rise. Sea level varies regionally due to factors including surface forcing, ocean circulation changes, thermal expansion of seawater, and melting of glacial ice.

Observational estimates of sea level changes during recent decades show substantial spatial variations (Figure S1a in Supporting Information S1). Future projections are also characterized by large spatial variations (Figure S1b in Supporting Information S1), although there is considerable uncertainty in the regional structure of projected sea level rise during the coming century (e.g., Couldrey et al., 2023; Gregory et al., 2016).

The melting of glacial ice influences global and regional sea level changes due to the volume added to the ocean, the effect of the freshwater flux on the ocean salinity, and the effect of latent heat of melting on the ocean temperature if the ice melts in the ocean (e.g., Church et al., 2013). Variations in the distribution of ice on land also influence regional sea level due to changes in the shape of the gravitational field of the Earth (e.g., Bamber et al., 2009; Gomez et al., 2010; Mitrovica et al., 2009).

The Antarctic Ice Sheet is the largest body of frozen ice on earth and contains enough ice to cause a global sea level rise of 60 m. Observational studies have found that the mass of the Antarctic Ice Sheet has decreased during recent decades (e.g., Bamber et al., 2018; Otosaka et al., 2023; Rignot et al., 2011, 2019; Smith et al., 2020; Velicogna & Wahr, 2013). This is associated with an increase in freshwater discharge into the ocean, which impacts global and regional sea level. Floating ice shelves around Antarctica have also been losing mass during recent decades (Paolo et al., 2015; Rignot et al., 2019; Shepherd et al., 2010). Model projections suggest that the

rate of ice mass loss in Antarctica will increase in the future, perhaps dramatically (e.g., DeConto & Pollard, 2016; Edwards et al., 2019; Joughin et al., 2014; Nick et al., 2013; Seroussi et al., 2020).

Freshwater fluxes into the ocean from glacial mass loss are not included in the comprehensive global climate model (GCM) simulations carried out for the Coupled Model Intercomparison Project Phase 5 (CMIP5) and Phase 6 (CMIP6) (Eyring et al., 2016; Taylor et al., 2011), which are used for the future projections in the IPCC Assessment Reports. These GCMs do not resolve ice sheet changes, instead typically representing ice sheets essentially as land with a thick snow cover and routing any excess snow accumulation back to the ocean. For example, in the CMIP5 model NCAR CCSM4, if snow accumulation reaches 1 m of snow water equivalent then any additional snowfall is added as runoff to the ocean surface net freshwater flux near the coast (Oleson et al., 2010).

Future sea level projections in the IPCC AR5 were created from CMIP5 simulation output as the sum of two non-interactive components (Church et al., 2013): (a) the ocean dynamic sea level field plus the global-mean sea level rise due to thermal expansion of the ocean, which is computed in each GCM, and (b) the sea level change from ice sheets, smaller glaciers, and terrestrial water, which is calculated using a separate modeling framework. The latter is forced by the global-mean temperature from the GCMs, and it accounts for the mass balance of the Antarctic and Greenland Ice Sheets and smaller glaciers, groundwater storage changes, and the regional influence of gravitational and rotational changes. Hence the sea level projection shown in Figure S1b in Supporting Information S1, which is equivalent to the projections used in the IPCC AR5, does not include the influence of glacial melt on ocean circulation and dynamic sea level changes. A similar approach is used in the IPCC AR6 based on CMIP6 simulation results.

Previous climate modeling studies that have explicitly included fluxes from Antarctic ice mass loss have typically treated them as part of the surface forcing of the ocean (e.g., Bronselaer et al., 2018; Golledge et al., 2019; Moorman et al., 2020; Park et al., 2023; Stammer, 2008; Stouffer et al., 2007). However, observational evidence suggests that the largest source of ablation in Antarctica is basal melt of ice shelves in contact with the ocean at depth, with a smaller contribution coming from iceberg calving (Depoorter et al., 2013; Rignot et al., 2013). Consistent with this, in situ measurements of the water column near an Antarctic ice shelf show that the meltwater is most concentrated near a depth of 0.5 km below the surface (Kim et al., 2016). Furthermore, in situ measurements from another study indicate that Antarctic glacial meltwater is often injected into the coastal ocean considerably deeper than the basal melt source due to overturning instability of the outflow from the ice shelf cavity (Garabato et al., 2017). Measurements such as these suggest that a substantial fraction of the meltwater fluxes associated with Antarctic ice mass loss should be applied at a depth greater than 0.5 km below the surface in model projections of sea level rise, since GCMs used for future projections normally do not simulate ice shelf ablation or cavity flow.

The regional sea level response to Antarctic ice melt may be expected to potentially depend on the depth of the forcing, because this forcing can trigger a range of depth-dependent baroclinic responses within the ocean. To this end, a study using satellite measurements together with an ocean model found considerable spatial structure of sea level changes near Antarctica associated with the vertical structure of temperature and salinity variations from the ablation of the ice shelves (Rye et al., 2014). Similarly, an ocean modeling study found that the simulated temperature and salinity along the continental shelf depends on whether Antarctic ice shelf melt fluxes are applied at the surface or at depth (Mathiot et al., 2017).

However, although some previous modeling studies have applied subsurface Antarctic ice shelf melt fluxes to study the response of the Southern Ocean stratification, sea ice cover, and pattern of sea surface temperature changes (Dong et al., 2022; Jeong et al., 2020; Mathiot et al., 2017; Merino et al., 2018; Pauling et al., 2016, 2017), there has been a paucity of previous work exploring model simulations of the global sea level response to subsurface ice melt forcing.

Improved understanding of the ocean response to subsurface fluxes from Antarctica can help reduce the uncertainty in the future ocean circulation and climate response to such perturbations. It may also help elucidate the role of sub-surface processes in triggering ice melt feedbacks that have been proposed in recent studies (Bronselaer et al., 2018; Golledge et al., 2019; Schmidtko et al., 2014; Si et al., 2023; Silvano et al., 2018). Here we use ocean GCM simulations in an idealized configuration in order to provide an initial proof-of-concept to demonstrate how the pattern of sea level rise depends on the depth of melt fluxes around Antarctica.

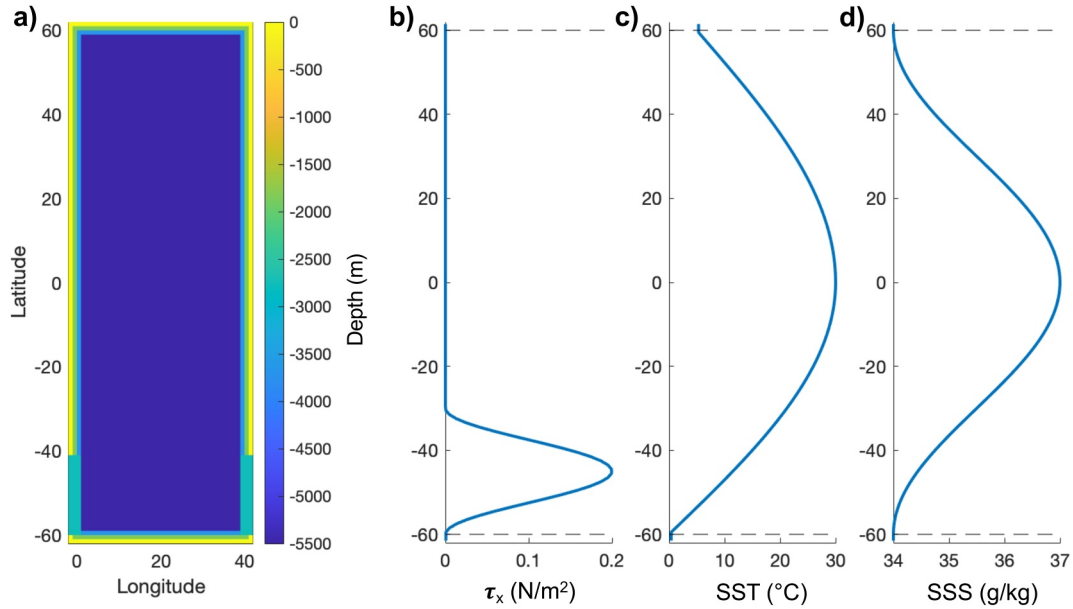

Figure 1. MITgcm simulation setup. (a) Basin bathymetry, including re-entrant Southern Ocean channel. (b) Specified zonal wind stress forcing. (c) Sea surface temperature relaxation field. (d) Sea surface salinity relaxation field. This setup is similar to Munday et al. (2013) but adopts a wider basin and adds continental shelves. During the Spin-up simulation, the temperature and salinity are relaxed to these fields. The relaxation conditions are replaced with specified surface fluxes during the Control and freshwater perturbation simulations, using a method adopted from Zika et al. (2018) and Todd et al. (2020).

2. Description of Simulations

The simulations were carried out with the Massachusetts Institute of Technology General Circulation Model (MITgcm: Marshall et al., 1997) setup in an idealized rectangular ocean basin bathymetry with a re-entrant channel in the Southern Ocean. We begin with a "Spin-up" simulation, in which we use surface temperature and salinity relaxation conditions with relaxation timescales of 10 and 30 days, respectively, as well as specified surface wind stress over the Southern Ocean. The basin configuration and forcing are shown in Figure 1. We adopt a relatively coarse horizontal resolution of 1°× 1°, using the Gent-McWilliams parameterization with an isopycnal thickness diffusivity and Redi isopycnal tracer diffusivity which are both set to 1,000 m^2s^{-1} to represent unresolved mesoscale eddies (Gent & McWilliams, 1990; Redi, 1982). We run the model with constant forcing, rather than including seasonal variations. We use idealized continental shelves along the basin edges, with the bathymetry decreasing linearly from a depth of 0 m to the basin depth of 5,500 m over 4°, with no-slip boundary conditions along the walls and bottom of the basin, and we use a channel depth of 2,750 m.

The simulations are described in more detail in Text S1 in Supporting Information S1. We branch the "Control," "Surface" freshwater perturbation, and "Deep" freshwater perturbation simulations from the approximately equilibrated state at the beginning of year 7540 of the Spin-up simulation (note that the simulations start at the beginning of year 0). These simulations have the temperature and salinity relaxation condition replaced by specified heat and salt fluxes, using a repeating 60-year cycle of daily fluxes that we save from years 7540 to 7599 of the Spin-up simulation. This follows the method of Zika et al. (2018) and Todd et al. (2020), allowing us to directly examine the response of the ocean to perturbations without damping by the atmosphere. The Control simulation has no freshwater perturbation and hence is similar to the Spin-up simulation, except that it has fixed surface fluxes rather than relaxation conditions. The Surface and Deep simulations have freshwater perturbations as described below. We run each of these three fixed-flux simulations for 240 years while also continuing the Spin-up simulation for 435 years to the end of year 7974.

Some previous studies of the ocean response to Antarctic ice melt have applied a horizontal structure of the meltwater flux that is uniform around the Antarctic coast (e.g., Bronselaer et al., 2018), others have scaled the observed pattern (e.g., Snow et al., 2016), and others have used more sophisticated representations such as scaling the linear trend of recent observed ice shelf thickness changes (Moorman et al., 2020). Each of these approaches

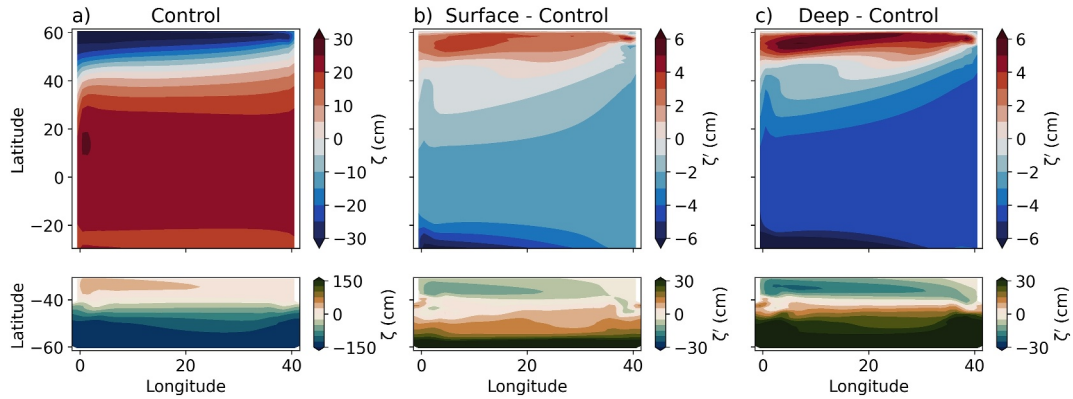

Figure 2. Simulated sea level. (a) Control simulation dynamic sea level ζ. (b) Surface freshwater perturbation simulation dynamic sea level anomaly from Control ζ'. (c) Deep freshwater perturbation simulation dynamic sea level anomaly from Control ζ'. The fields are averaged over the last decade of each of the 240-year simulations. Note the differing color scales between the upper and lower panels.

has strengths and weaknesses. Using a horizontally uniform forcing is simple and hence conducive to building conceptual understanding, but it may miss key features of the horizontal structure of the ice melt forcing. Scaling observed fluxes could be more accurate, but the fluxes from ice shelves with the largest basal melt rates today will not necessarily increase the most in the future. Amplifying observed ice shelf thickness changes may better capture these sensitivities, but the observational record may be too short to separate interannual variability in basal melt from secular trends, and ice shelf thickness changes do not directly map to basal melt changes due to factors including changes in ice flow across the grounding line (e.g., Adusumilli et al., 2020).

In the present study, we apply meltwater fluxes in zonally uniform bands along the southern border of the basin (60°S), with the aim of providing a first step toward understanding how the sea level adjustment depends on the depth of the flux. The Surface simulation has a 0.1 Sv freshwater flux applied at the surface, and the Deep simulation has a 0.1 Sv freshwater flux applied at a depth of 1 km. The fluxes are held constant throughout the simulations. We do not include cooling from the latent heat of ice shelf melting (See Text S1 in Supporting Information S1 for further details). This 0.1 Sv flux is similar to the Antarctic Ice Sheet meltwater discharge rates in some projections. Edwards et al. (2019) report an 83 cm Antarctic contribution to sea level during 2000–2100, and DeConto and Pollard (2016) similarly report a 105 cm Antarctic contribution to sea level during 2000–2100, where in both cases we are citing the highest reported scenarios, which use RCP8.5 forcing and include the marine ice cliff instability. These amount to century-averaged freshwater inputs of 0.091 and 0.12 Sv, respectively. The DeConto and Pollard (2016) ice sheet simulation has similarly been used for the forcing in a number of other ocean modeling studies (e.g., Bronselaer et al., 2018; Lago & England, 2019; Schloesser et al., 2019). Note that this imposed 0.1 Sv flux anomaly is about twice as large as the basal melt component of the Antarctic Ice Sheet mass balance in the current climate, which is estimated by to be 1,325 gigatons per year (Rignot et al., 2013), amounting to a freshwater flux of 0.042 Sv. Much of this observed basal melt is balanced by other terms in the ice sheet mass budget, however, rather than contributing to sea level rise (e.g., Slater et al., 2021).

Estimates of future Antarctic meltwater flux anomalies are subject to uncertainty in the ice sheet model physics, including the hypothesized marine ice cliff instability process, as well as uncertainty in the future radiative forcing scenario. Here we adopt a value on the high side of the uncertainty range in order to emphasize the possible sensitivity to meltwater depth.

3. Results

We focus on the ocean dynamic sea level ζ, which is the regional pattern of sea surface height; it is defined as the departure from the geoid, with a global-mean value of zero. This is equivalent to the MITgcm output variable "Eta" with the global-mean value removed. Note that ζ is reported in CMIP5 and CMIP6 as the simulation output variable "zos."

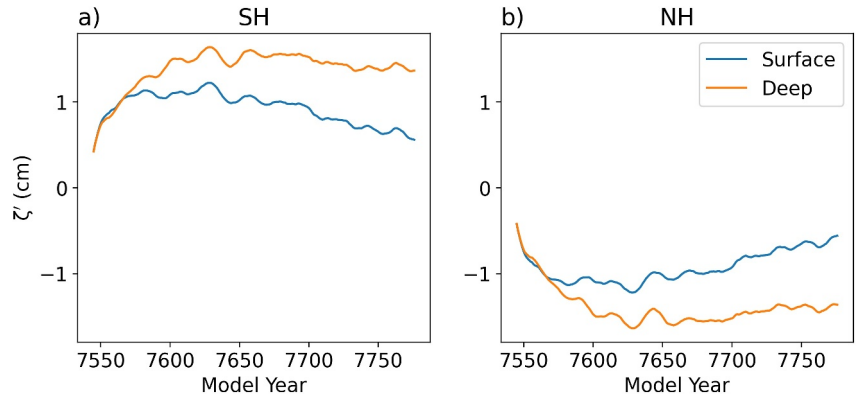

Figure 3. Time series of dynamic sea level anomaly from the Control simulation, ζ', in the Surface and Deep simulations. (a) Southern Hemisphere spatial mean. (b) Northern Hemisphere spatial mean. All curves are smoothed with a 10-year running mean.

The dynamic sea level ζ in the Control simulation is shown in Figure 2a. It is positive at latitudes equatorward of about 40°N and 40°S and negative at higher latitudes, which qualitatively resembles the observed global ocean (e.g., Mulet et al., 2021, their Figure 6a). Note, however, that the model configuration adopted here does not have wind-driven gyres, because the wind stress is zero outside the Southern Ocean channel.

The dynamic sea level anomalies from the Control simulations, ζ', are plotted for the Surface and Deep simulations in Figures 2b and 2c. The constant freshwater fluxes applied at the southern edge of the basin in both simulations leads to a higher regional sea level in southern high latitudes, and it broadly causes a reduction in the amplitude of the spatial pattern of ζ in the Control simulation. The key difference between the two simulations is that after the first couple decades, ζ' remains lower in the Northern Hemisphere and higher in the Southern Hemisphere in the Deep simulation, indicating that the applied freshwater flux spreads more slowly across the ocean basin.

This can be seen clearly in line plots of ζ' averaged spatially over each hemisphere (Figure 3). Averaged over the final 200 years of the simulations, ζ' is 2.9 cm higher in the Southern Hemisphere than in the Northern Hemisphere in the Deep simulation, compared with just 1.8 cm in the Surface simulation. Note that since ζ is defined to have a global-mean value of zero, the value in the Northern Hemisphere is equal and opposite to the value in the Southern Hemisphere. This result can be seen in more detail using Hovmöller plots that effectively combine Figures 2 and 3 (Figure S4 in Supporting Information S1). The sea level rise field is more globally uniform in the Surface simulation, as indicated by the smaller magnitudes of the values of ζ' in Figure S4a in Supporting information S1 (Surface simulation) compared with Figure S4b in Supporting information S1 (Deep simulation).

The results in Figures 2 and 3 show that the global sea level change pattern depends critically on the depth of the Antarctic meltwater perturbation, with far field sea level differences that persist throughout the simulations. Broadly, the elevated regional sea level moves more slowly out of the Southern Hemisphere when the freshwater is injected at depth.

4. Sea Level Change Decomposition

The dynamic sea level pattern in each perturbed simulation (Surface or Deep) can be decomposed as follows (e.g., Gill & Niiler, 1973; Gregory et al., 2019; Griffies et al., 2014; Yin et al., 2010):

$$\zeta' = \underbrace{\frac{p_b'}{\rho_0\, g}}_{\text{Mass}} \underbrace{- \frac{1}{\rho_0} \int_{-H}^{\zeta - B} \rho'\, dz}_{\text{Steric}}, \tag{1}$$

where ρ is the ocean density field, ρ_0 is the ocean reference density, g is the acceleration of gravity, p_b is the ocean bottom hydrostatic pressure, H is the ocean depth, and B represents the inverse barometer correction due to variations in sea level pressure (adopting the terminology of Gregory et al., 2019). Here primed quantities

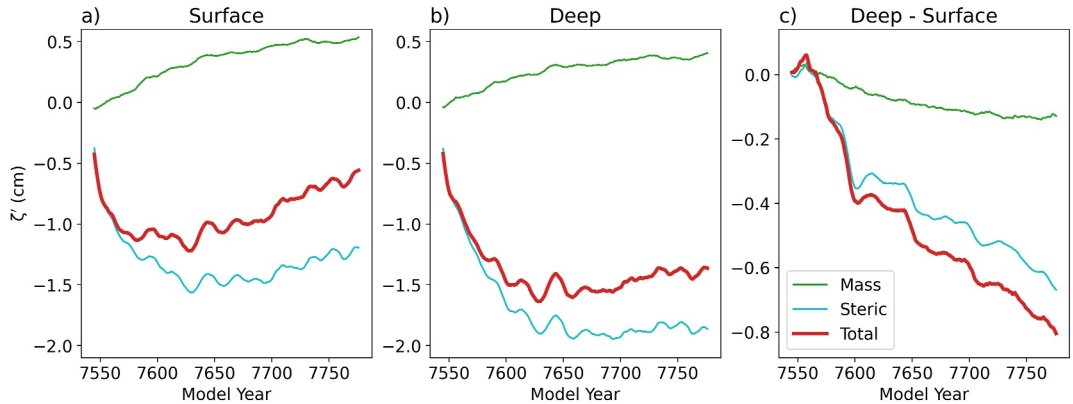

Figure 4. Decomposition of Northern Hemisphere dynamic sea level anomaly ζ' into mass redistribution and steric contributions (Equation 1). (a) Surface simulation. (b) Deep simulation. (c) Difference between the two simulations. All curves are smoothed with a 10-year running mean.

represent the anomaly in a perturbed simulation relative to the Control simulation, with the global mean removed. Note that Equation 1 is derived from the hydrostatic balance with the near-surface density approximated to be ρ_0 (e.g., Yin et al., 2010, their Section 2b).

The first term on the right-hand side of Equation 1 captures sea level increases due to seawater being added to the column, that is, it represents ocean mass redistribution. The second term on the right-hand side of Equation 1 captures sea level increases due to the column becoming less dense without changing its mass, that is, it represents the sea level change from local steric changes in the density field.

The terms in Equation 1 can be readily computed from the MITgcm simulation output. The left-hand side is the difference in the dynamic sea level ζ between the perturbed simulation and the Control simulation. The mass term is computed using the hydrostatic relationship as the difference between the simulations in the quantity $\frac{1}{\rho_0}\int_{-H}^{\eta}\rho\, dz$; the global mean is removed after calculating this term for each simulation. Since the surface pressure is constant in the MITgcm simulations, we take $B = 0$, and the steric term is computed as $-\frac{1}{\rho_0}\int_{-H}^{\zeta}\rho'\, dz$, with ρ' defined as above and ζ the dynamic sea level in the perturbed simulation.

The resulting quantities, averaged over the Northern Hemisphere, are plotted in Figure 4. The freshwater injection causes an increase in mass, which leads to a positive contribution to local sea level from the mass term in Equation 1 in southern high latitudes. This increase in sea level is further enhanced by the column becoming less dense due to the reduction in salinity from the freshwater injection, which leads to a positive contribution to local sea level from the steric term in Equation 1 in southern high latitudes. The hemispheric contrast in density driven by the freshwater injection explains most of the dynamic sea level anomaly ζ' (steric term in Figure 4). On the other hand, there is a rapid barotropic circulation response to the local increase in sea level in southern high latitudes, which causes the sea level to become more spatially uniform throughout the basin. In both perturbed simulations, the circulation response ultimately causes the ocean mass to increase more in the Northern Hemisphere than the Southern Hemisphere, which is indicated by the positive but relatively small value of the mass term in the Northern Hemisphere ζ' decomposition in Figure 4. Note that the mass term would dominate the Northern Hemisphere sea level change if the global mean were not removed (cf. Lorbacher et al., 2012).

The mass term in Equation 1 is approximately associated with the barotropic component of the flow, and the steric term is approximately associated with the baroclinic component of the flow (e.g., Savage et al., 2017). Indeed, explicitly decomposing the sea level changes into components associated with the barotropic and baroclinic components of the flow, following the method of McWilliams et al. (2024), leads to qualitatively similar results (Figure S5 in Supporting Information S1).

The relatively small value of the mass term (Figures 4a and 4b) and similarly the barotropic term (Figures S5a and S5b in Supporting Information S1) indicates that this component of the dynamic sea level anomaly ζ' spreads rapidly around the basin and hence has an approximately spatially uniform effect. This is consistent with the expectation that the barotropic response of sea level to mass injection propagates across the globe in a matter of

days to weeks (Lorbacher et al., 2012). The larger value of the steric term (Figures 4a and 4b) and similarly the baroclinic term (Figures S5a and S5b in Supporting Information S1) indicates that this component spreads more slowly, which is consistent with the expectation that the steric adjustment of the dynamic sea level arising from meltwater-induced changes in salinity propagates across the globe on far slower timescales of many decades or more (Stammer, 2008). In other words, although the mass from the injected freshwater spreads quickly into the Northern Hemisphere in both simulations due to the rapid propagation of barotropic waves (near-zero values of the green curves in Figures 4a and 4b), the density change from the injected freshwater spreads more slowly due to the slower baroclinic adjustment (substantial negative values of the blue curves in Figures 4a and 4b and Figures S4a and S4b in Supporting Information S1). This is especially the case in the Deep simulation: the steric component of the dynamic sea level anomaly ζ' spreads less into the Northern Hemisphere in the Deep simulation than in the Surface simulation during the simulated 240-year period (Figures 4a and 4b and Figures S4a and S4b in Supporting Information S1).

Additional details can be gleaned from examining the temperature, salinity, and density fields in the simulations. Compared with the Control simulation, the Surface simulation is colder and fresher near the ocean surface across the basin (Figures S6b and S6e in Supporting Information S1). This result is expected due to the cold fresh water being injected at the surface at the southern edge and propagating across the basin. The Deep simulation shows similar behavior, although the salinity anomaly (Figure S6f in Supporting Information S1) and the negative density anomaly (Figure S6i in Supporting Information S1) are more concentrated near the freshwater source, consistent with the steric response being more concentrated in the Southern Hemisphere (Figure 4). Note that the model simulates convective adjustment by applying vertical diffusion between any statically unstable cells (using a diffusivity of 1 m^2/s). The injection of 0°C freshwater at 1 km is expected to influence the static stability of the column, causing more vertical mixing above and less below. Consistent with this, the Deep simulation has anomalously fresh water extending from a depth of 1 km up to the surface in southern high latitudes, with an increase in salinity and temperature at greater depths as expected from less mixing downward of the colder and fresher waters that are higher in the water column. Similarly, the Surface simulation has anomalously fresh water concentrated near the surface in southern high latitudes, with an increase in temperature in the column below.

The circulation is also influenced by the freshwater perturbations. The residual meridional overturning circulation in the Control run features an upper and lower cell, in approximate qualitative agreement with observations (Figure S7a in Supporting Information S1). The freshwater perturbation in the Deep simulation causes the lower cell to shift downward, such that it no longer outcrops in the Southern Ocean and remains below ∼1 km (Figure S7c in Supporting Information S1), although the circulation at depths greater than ∼1 km remains qualitatively unchanged. The freshwater perturbation in the Surface simulation causes the lower cell to nearly shut off (Figure S7b in Supporting Information S1). These changes in the circulation are expected to also influence the density field (Figures S6h and S6i in Supporting Information S1) and hence the steric response (Figure 4).

5. Summary and Conclusions

Previous climate modeling studies that have explicitly included fluxes from Antarctic ice mass loss have typically treated them as part of the surface forcing of the ocean. However, observational estimates suggest that the largest source of ablation in Antarctica is basal melt of ice shelves, with the freshwater entering the ocean considerably below the surface. In the present study, we use MITgcm simulations of an idealized ocean basin with freshwater injected at the surface or at depth in southern high latitudes. The results suggest that the global sea level change pattern is sensitive to the depth of the Antarctic meltwater perturbation. When the fluxes are applied at depth the signal tends to travel more slowly to the Northern Hemisphere. This is consistent with expectations that the propagation speeds of baroclinic waves will depend on the stratification, which is influenced by the depth of the meltwater injection. A decomposition of the sea level changes shows that the sensitivity to meltwater depth occurs primarily due to differences in the baroclinic response.

Many factors have been neglected in these idealized simulations, including but not limited to the influence of realistic basin geometry, the detailed spatial and temporal structure of the meltwater injection, and the latent heat flux in addition to freshwater injection associated with ice shelf basal melt. Each of these factors could play an important role in determining the pattern of sea level changes. For example, the latent heat flux cools the ocean and hence may be expected to oppose the effect of freshening on the water density. Further research into how these factors would influence these results is called for. The simulations were carried out with a 1° GCM, raising

important questions about how the results may differ in a higher-resolution model. Seasonal variations are omitted, which may be expected to play an important role in the vertical mixing of freshwater anomalies in the Southern Ocean. Also, freshwater anomalies influence sea ice formation, which influences the vertical mixing in the ocean below, and these simulations omit sea ice. Furthermore, the scale of the regional patterns of change in the simulation results (Figure 2c), while of a similar order of magnitude to the projected regional pattern of sea level rise during the coming century (Figure S1 in Supporting Information S1), would be considerably smaller than the global-mean sea level rise due to substantial Antarctic Ice Sheet melting and associated feedbacks. This is true in general for local patterns of dynamic sea level compared to global mean sea level change. Nonetheless, the results presented here suggest that sea level changes are sensitive to the depth of freshwater injections, which suggests that capturing the depth of Antarctic ice shelf meltwater may lead to more accurate projections of future regional sea level changes, in particular when considering local impacts such as increased risk of flooding and storm surge.

Data Availability Statement

The MITgcm simulation output and analysis code to generate the figures in this paper are available online (Eisenman et al., 2024).

Acknowledgments
Without implying their endorsement of our results, we thank Stephen Griffies, Jake Steinberg, Geoff Vallis, Ruth Moorman, and two anonymous reviewers for helpful comments. This work was supported by National Science Foundation Grants OCE-2048590 and OCE-2048576.

References

Adusumilli, S., Fricker, H. A., Medley, B., Padman, L., & Siegfried, M. R. (2020). Interannual variations in meltwater input to the Southern Ocean from Antarctic ice shelves. *Nature Geoscience*, *13*(9), 191–194. https://doi.org/10.1038/s41561-020-0616-z

Bamber, J. L., Riva, R. E. M., Vermeersen, B. L. A., & LeBrocq, A. M. (2009). Reassessment of the potential sea-level rise from a collapse of the west Antarctic ice sheet. *Science*, *324*(5929), 901–903. https://doi.org/10.1126/science.1169335

Bamber, J. L., Westaway, R. M., Marzeion, B., & Wouters, B. (2018). The land ice contribution to sea level during the satellite era. *Environmental Research Letters*, *13*(9), 063008. https://doi.org/10.1088/1748-9326/aadb2c

Bronselaer, B., Winton, M., Griffies, S. M., Hurlin, W. J., Rodgers, K. B., Sergienko, O. V., et al. (2018). Change in future climate due to Antarctic meltwater. *Nature*, *564*(7734), 53–58. https://doi.org/10.1038/s41586-018-0712-z

Church, J., Clark, P., Cazenave, A., Gregory, J., Jevrejeva, S., Levermann, A., et al. (2013). Chapter 13, Sea level change. In T. Stocker, et al. (Eds.), *Climate Change 2013: The Physical Science Basis. Contribution of Working Group I to the Fifth Assessment Report of the Intergovernmental Panel on Climate Change*. Cambridge University Press.

Couldrey, M. P., Gregory, J. M., Dong, X., Garuba, O., Haak, H., Hu, A. X., et al. (2023). Greenhouse-gas forced changes in the Atlantic meridional overturning circulation and related worldwide sea-level change. *Climate Dynamics*, *60*(7–8), 2003–2039. https://doi.org/10.1007/s00382-022-06386-y

DeConto, R. M., & Pollard, D. (2016). Contribution of Antarctica to past and future sea-level rise. *Nature*, *531*(7596), 591–597. https://doi.org/10.1038/nature17145

Depoorter, M. A., Bamber, J. L., Griggs, J. A., Lenaerts, J. T. M., Ligtenberg, S. R. M., van den Broeke, M. R., & Moholdt, G. (2013). Calving fluxes and basal melt rates of Antarctic ice shelves. *Nature*, *502*(7469), 89–92. https://doi.org/10.1038/nature12567

Dong, Y., Pauling, A. G., Sadai, S., & Armour, K. C. (2022). Antarctic ice-sheet meltwater reduces transient warming and climate sensitivity through the sea-surface temperature pattern effect. *Geophysical Research Letters*, *49*(24), e2022GL101249. https://doi.org/10.1029/2022GL101249

Edwards, T. L., Brandon, M. A., Durand, G., Edwards, N. R., Golledge, N. R., Holden, P. B., et al. (2019). Revisiting Antarctic ice loss due to marine ice-cliff instability. *Nature*, *566*(7742), 58–64. https://doi.org/10.1038/s41586-019-0901-4

Eisenman, I., Basinski-Ferris, A., Beer, E., & Zanna, L. (2024). MITgcm simulations of sea level response to freshwater injected at the surface and at depth in southern high latitudes: Model output and analysis code. *Zenodo*. https://doi.org/10.5281/zenodo.13766600

Eyring, V., Bony, S., Meehl, G. A., Senior, C. A., Stevens, B., Stouffer, R. J., & Taylor, K. E. (2016). Overview of the coupled model intercomparison project phase 6 (CMIP6) experimental design and organization. *Geoscientific Model Development*, *9*(5), 1937–1958. https://doi.org/10.5194/gmd-9-1937-2016

Garabato, A. C. N., Forryan, A., Dutrieux, P., Brannigan, L., Biddle, L. C., Heywood, K. J., et al. (2017). Vigorous lateral export of the meltwater outflow from beneath an Antarctic ice shelf. *Nature*, *542*(7640), 219–222. https://doi.org/10.1038/nature20825

Gent, P. R., & McWilliams, J. C. (1990). Isopycnal mixing in ocean circulation models. *Journal of Physical Oceanography*, *20*(1), 150–155. https://doi.org/10.1175/1520-0485(1990)020⟨0150:IMIOCM⟩2.0.CO;2

Gill, A. E., & Niiler, P. P. (1973). Theory of seasonal variability in ocean. *Deep Sea Research*, *20*(2), 141–177. https://doi.org/10.1016/0011-7471(73)90049-1

Golledge, N. R., Keller, E. D., Gomez, N., Naughten, K. A., Bernales, J., Trusel, L. D., & Edwards, T. L. (2019). Global environmental consequences of twenty-first-century ice-sheet melt. *Nature*, *566*(7742), 65–72. https://doi.org/10.1038/s41586-019-0889-9

Gomez, N., Mitrovica, J. X., Huybers, P., & Clark, P. U. (2010). Sea level as a stabilizing factor for marine-ice-sheet grounding lines. *Nature Geoscience*, *3*(12), 850–853. https://doi.org/10.1038/NGEO1012

Gregory, J., Bouttes, N., Griffies, S. M., Haak, H., Hurlin, W. J., Jungclaus, J., et al. (2016). The flux-anomaly-forced model intercomparison project (FAFMIP) contribution to CMIP6: Investigation of sea-level and ocean climate change in response to CO_2 forcing. *Geoscientific Model Development*, *9*(11), 3993–4017. https://doi.org/10.5194/gmd-9-3993-2016

Gregory, J., Griffies, S., Hughes, C., Lowe, J., Church, J., Fukimori, I., et al. (2019). Concepts and terminology for sea level: Mean, variability and change, both local and global. *Surveys in Geophysics*, *40*(6), 1–39. https://doi.org/10.1007/s10712-019-09525-z

Griffies, S. M., Yin, J. J., Durack, P. J., Goddard, P., Bates, S. C., Behrens, E., et al. (2014). An assessment of global and regional sea level for years 1993–2007 in a suite of interannual CORE-II simulations. *Ocean Modelling*, *78*, 35–89. https://doi.org/10.1016/j.ocemod.2014.03.004

Jeong, H., Asay-Davis, X. S., Turner, A. K., Comeau, D. S., Price, S. F., Abernathey, R. P., et al. (2020). Impacts of ice-shelf melting on water-mass transformation in the southern ocean from E3SM simulations. *Journal of Climate*, *33*(13), 5787–5807. https://doi.org/10.1175/JCLI-D-19-0683.1

Jevrejeva, S., Jackson, L. P., Grinsted, A., Lincke, D., & Marzeion, B. (2018). Flood damage costs under the sea level rise with warming of 1.5°C and 2°C. *Environmental Research Letters*, *13*(7), 074014. https://doi.org/10.1088/1748-9326/aacc76

Joughin, I., Smith, B. E., & Medley, B. (2014). Marine ice sheet collapse potentially under way for the Thwaites Glacier Basin, West Antarctica. *Science*, *344*(6185), 735–738. https://doi.org/10.1126/science.1249055

Kim, I., Hahm, D., Rhee, T. S., Kim, T. W., Kim, C. S., & Lee, S. (2016). The distribution of glacial meltwater in the Amundsen Sea, Antarctica, revealed by dissolved helium and neon. *Journal of Geophysical Research: Oceans*, *121*(3), 1654–1666. https://doi.org/10.1002/2015JC011211

Lago, V., & England, M. H. (2019). Projected slowdown of Antarctic Bottom Water formation in response to amplified meltwater contributions. *Journal of Climate*, *32*(19), 6319–6335. https://doi.org/10.1175/JCLI-D-18-0622.1

Lorbacher, K., Marsland, S. J., Church, J. A., Griffies, S. M., & Stammer, D. (2012). Rapid barotropic sea level rise from ice sheet melting. *Journal of Geophysical Research*, *117*(C6), C06003. https://doi.org/10.1029/2011JC007733

Marshall, J., Adcroft, A., Hill, C., Perelman, L., & Heisey, C. (1997). A finite-volume, incompressible Navier Stokes model for studies of the ocean on parallel computers. *Journal of Geophysical Research*, *102*(C3), 5753–5766. https://doi.org/10.1029/96JC02775

Mathiot, P., Jenkins, A., Harris, C., & Madec, G. (2017). Explicit representation and parametrised impacts of under ice shelf seas in the z* coordinate ocean model NEMO 3.6. *Geoscientific Model Development*, *10*(7), 2849–2874. https://doi.org/10.5194/gmd-10-2849-2017

McWilliams, J. C., Molemaker, M. J., & Damien, P. (2024). Baroclinic sea level. *Journal of Advances in Modeling Earth Systems*, *16*(4), e2023MS003977. https://doi.org/10.1029/2023MS003977

Merino, N., Jourdain, N. C., Sommer, J. L., Goosse, H., Mathiot, P., & Durand, G. (2018). Impact of increasing Antarctic glacial freshwater release on regional sea-ice cover in the Southern Ocean. *Ocean Modelling*, *121*, 76–89. https://doi.org/10.1016/j.ocemod.2017.11.009

Mitrovica, J. X., Gomez, N., & Clark, P. U. (2009). The sea-level fingerprint of West Antarctic collapse. *Science*, *323*(5915), 753. https://doi.org/10.1126/science.1166510

Moorman, R., Morrison, A., & Hogg, A. (2020). Thermal responses to Antarctic Ice Shelf melt in an eddy-rich global ocean-sea ice model. *Journal of Climate*, *33*(15), 6599–6620. https://doi.org/10.1175/JCLI-D-19-0846.1

Mulet, S., Rio, M.-H., Etienne, H., Artana, C., Cancet, M., Dibarboure, G., et al. (2021). The new CNES-CLS18 global mean dynamic topography. *Ocean Science*, *17*(3), 789–808. https://doi.org/10.5194/os-17-789-2021

Munday, D. R., Johnson, H. L., & Marshall, D. P. (2013). Eddy saturation of equilibrated circumpolar currents. *Journal of Physical Oceanography*, *43*(3), 507–532. https://doi.org/10.1175/JPO-D-12-095.1

Nick, F. M., Vieli, A., Andersen, M. L., Joughin, I., Payne, A., Edwards, T. L., et al. (2013). Future sea-level rise from Greenland's main outlet glaciers in a warming climate. *Nature*, *497*(7448), 235–238. https://doi.org/10.1038/nature12068

Oleson, K. W., Lawrence, D. M., Bonan, G. B., Flanner, M. G., Kluzek, E., Lawrence, P. J., et al. (2010). Technical description of version 4.0 of the community land model (clm) [Computer software manual]. *National Center for Atmospheric Research*. Retrieved from http://www.cesm.ucar.edu/models/cesm2/land/CLM50_Tech_Note.pdf

Otosaka, I. N., Shepherd, A., Ivins, E. R., Schlegel, N. J., Amory, C., van den Broeke, M. R., et al. (2023). Mass balance of the Greenland and Antarctic ice sheets from 1992 to 2020. *Earth System Science Data*, *15*(4), 1597–1616. https://doi.org/10.5194/essd-15-1597-2023

Paolo, F. S., Fricker, H. A., & Padman, L. (2015). Volume loss from Antarctic ice shelves is accelerating. *Science*, *348*(6232), 327–331. https://doi.org/10.1126/science.aaa0940

Park, J. Y., Schloesser, F., Timmermann, A., Choudhury, D., Lee, J. Y., & Nellikkattil, A. B. (2023). Future sea-level projections with a coupled atmosphere-ocean-ice-sheet model. *Nature Communications*, *14*(1), 636. https://doi.org/10.1038/s41467-023-36051-9

Pauling, A. G., Bitz, C. M., Smith, I. J., & Langhorne, P. J. (2016). The response of the Southern Ocean and Antarctic sea ice to freshwater from ice shelves in an Earth system model. *Journal of Climate*, *29*(5), 1655–1672. https://doi.org/10.1175/JCLI-D-15-0501.1

Pauling, A. G., Smith, I. J., Langhorne, P. J., & Bitz, C. M. (2017). Time-dependent freshwater input from ice shelves: Impacts on Antarctic sea ice and the Southern Ocean in an Earth system model. *Geophysical Research Letters*, *44*(20), 10454–10461. https://doi.org/10.1002/2017GL075017

Redi, M. H. (1982). Oceanic isopycnal mixing by coordinate rotation. *Journal of Physical Oceanography*, *12*(10), 1154–1158. https://doi.org/10.1175/1520-0485(1982)012⟨1154:OIMBCR⟩2.0.CO;2

Rignot, E., Jacobs, S., Mouginot, J., & Scheuchl, B. (2013). Ice-shelf melting around Antarctica. *Science*, *341*(6143), 266–270. https://doi.org/10.1126/science.1235798

Rignot, E., Mouginot, J., Scheuchl, B., van den Broeke, M., van Wessem, M. J., & Morlighem, M. (2019). Four decades of Antarctic ice sheet mass balance from 1979–2017. *Proceedings of the National Academy of Sciences of the United States of America*, *116*(4), 1095–1103. https://doi.org/10.1073/pnas.1812883116

Rignot, E., Velicogna, I., van den Broeke, M. R., Monaghan, A., & Lenaerts, J. (2011). Acceleration of the contribution of the Greenland and Antarctic ice sheets to sea level rise. *Geophysical Research Letters*, *38*(5), L05503. https://doi.org/10.1029/2011GL046583

Rye, C. D., Garabato, A. C. N., Holland, P. R., Meredith, M. P., Nurser, A. J. G., Hughes, C. W., et al. (2014). Rapid sea-level rise along the Antarctic margins in response to increased glacial discharge. *Nature Geoscience*, *7*(10), 732–735. https://doi.org/10.1038/NGEO2230

Savage, A. C., Arbic, B. K., Richman, J. G., Shriver, J. F., Alford, M. H., Buijsman, M. C., et al. (2017). Frequency content of sea surface height variability from internal gravity waves to mesoscale eddies. *Journal of Geophysical Research: Oceans*, *122*(3), 2519–2538. https://doi.org/10.1002/2016JC012331

Schloesser, F., Friedrich, T., Timmermann, A., DeConto, R. M., & Pollard, D. (2019). Antarctic iceberg impacts on future Southern Hemisphere climate. *Nature Climate Change*, *9*(9), 672–677. https://doi.org/10.1038/s41558-019-0546-1

Schmidtko, S., Heywood, K. J., Thompson, A. F., & Aoki, S. (2014). Multidecadal warming of Antarctic waters. *Science*, *346*(6214), 1227–1231. https://doi.org/10.1126/science.1256117

Seroussi, H., Nowicki, S., Payne, A. J., Goelzer, H., Lipscomb, W. H., Abe Ouchi, A., et al. (2020). ISMIP6 Antarctica: A multi-model ensemble of the Antarctic ice sheet evolution over the 21st century. *The Cryosphere Discussions*, *2020*, 1–54. https://doi.org/10.5194/tc-2019-324

Shepherd, A., Wingham, D., Wallis, D., Giles, K., Laxon, S., & Sundal, A. V. (2010). Recent loss of floating ice and the consequent sea level contribution. *Geophysical Research Letters*, *37*(13), L13503. https://doi.org/10.1029/2010GL042496

Si, Y. D. F., Stewart, A. L., & Eisenman, I. (2023). Heat transport across the Antarctic Slope Front controlled by cross-slope salinity gradients. *Science Advances*, *9*(18), eadd7049. https://doi.org/10.1126/sciadv.add7049

Silvano, A., Rintoul, S. R., Pena-Molino, B., Hobbs, W. R., van Wijk, E., Aoki, S., et al. (2018). Freshening by glacial meltwater enhances melting of ice shelves and reduces formation of Antarctic Bottom Water. *Science Advances*, *4*(4), eaap9467. https://doi.org/10.1126/sciadv.aap9467

Slater, T., Lawrence, I. R., Otosaka, I. N., Shepherd, A., Gourmelen, N., Jakob, L., et al. (2021). Review article: Earth's ice imbalance. *The Cryosphere*, *15*(1), 233–246. https://doi.org/10.5194/tc-15-233-2021

Smith, B., Fricker, H. A., Gardner, A. S., Medley, B., Nilsson, J., Paolo, F. S., et al. (2020). Pervasive ice sheet mass loss reflects competing ocean and atmosphere processes. *Science*, *368*(6496), 1239–1242. https://doi.org/10.1126/science.aaz5845

Snow, K., Hogg, A. M., Sloyan, B. M., & Downes, S. M. (2016). Sensitivity of Antarctic bottom water to changes in surface buoyancy fluxes. *Journal of Climate*, *29*(1), 313–330. https://doi.org/10.1175/JCLI-D-15-0467.1

Stammer, D. (2008). Response of the global ocean to Greenland and Antarctic ice melting. *Journal of Geophysical Research*, *113*(C6), C06022. https://doi.org/10.1029/2006JC004079

Stouffer, R. J., Seidov, D., & Haupt, B. J. (2007). Climate response to external sources of freshwater: North Atlantic versus the Southern Ocean. *Journal of Climate*, *20*(3), 436–448. https://doi.org/10.1175/JCLI4015.1

Taylor, K. E., Stouffer, R. J., & Meehl, G. A. (2011). An overview of CMIP5 and the experiment design. *Bulletin America Meteorology Social*, *93*(4), 485–498. https://doi.org/10.1175/BAMS-D-11-00094.1

Todd, A., Zanna, L., Couldrey, M., Gregory, J., Wu, Q., Church, J. A., et al. (2020). Ocean-only FAFMIP: Understanding regional patterns of ocean heat content and dynamic sea level change. *Journal of Advances in Modeling Earth Systems*, *12*(8), e2019MS002027. https://doi.org/10.1029/2019MS002027

Velicogna, I., & Wahr, J. (2013). Time-variable gravity observations of ice sheet mass balance: Precision and limitations of the GRACE satellite data. *Geophysical Research Letters*, *40*(12), 3055–3063. https://doi.org/10.1002/grl.50527

Yin, J. J., Griffies, S. M., & Stouffer, R. J. (2010). Spatial variability of sea level rise in twenty-first century projections. *Journal of Climate*, *23*(17), 4585–4607. https://doi.org/10.1175/2010JCLI3533.1

Zika, J. D., Skliris, N., Blaker, A. T., Marsh, R., Nurser, A. J. G., & Josey, S. A. (2018). Improved estimates of water cycle change from ocean salinity: The key role of ocean warming. *Environmental Research Letters*, *13*(7), 074036. https://doi.org/10.1088/1748-9326/aace42

Supporting Information S1 for "The sensitivity of the spatial pattern of sea level changes to the depth of Antarctic meltwater fluxes"

Ian Eisenman, Aurora Basinski-Ferris, Emma Beer, and Laure Zanna

Contents of this file

Text S1: Description of simulation

We initially run the model for 300 years. We then test the sensitivity of model parameters that control mixing, diffusion, and convection, and we adjust the parameters in order to simulate a relatively realistic ocean circulation including the global residual meridional overturning circulation. Specifically, we change the parameters "diffKrNrT" and "diffKrNrS", which are the background vertical diffusivity profiles for temperature and salinity and are set equal to each other in these simulations. The default profile during the sensitivity testing and the adjusted profile used in the Spin-up simulation (and equivalently the meltwater perturbation simulations) are shown in Fig. S8.

We then run the Spin-up simulation until the end of year 7974. We find that the global volume-mean temperature and salinity evolve approximately exponentially toward their equilibrium values with e-folding timescales of 1090 years and 1340 years, respectively, after the first few thousand years (Fig. S2).

The Control, Surface, and Deep simulations are branched from the beginning of year 7540 of the Spin-up simulation. We set the Spin-up simulation to save daily output of the temperature and salinity relaxation fields during years 7540-7599, which we use to generate a 60-year cycle of daily fluxes. Note that the simulations with specified fluxes use the "Qnet" and "saltflux" surface forcing options in MITgcm. This requires changing the sign of the Spin-up simulation output to be used as input in the simulations with specified fluxes. In order to preserve the daily-mean values when the model linearly interpolates between values at the midpoint of each day, we use a process called "diddling" to adjust the daily data (Killworth, 1996). The perturbations in the Surface and Deep simulations are added as water at 0 psu and 0°C using the "AddMass" option in MITgcm. Note that this setup treats evaporation and precipitation at the surface as a virtual salt flux, whereas it treats injected glacial meltwater as a real freshwater flux.

We select year 7540 as the start time of the simulations with specified fluxes because (i) it allows the Spin-up simulation to reach a relatively high level of equilibration (SI Fig. S2) and (ii) the 60-year mean during years 7540–7599 of the global means of both flux fields is approximately zero (SI Fig. S3). The latter condition is important because the global volume-mean temperature and salinity in the Control simulation evolves at a constant rate that is set by the global-mean values of these fixed surface fluxes. The drift in volume-mean temperature and salinity in the Control simulation is 2.5×10^{-5} K/yr and 7×10^{-6} g/kg/yr, which is considerably smaller than some other studies that used a similar method (e.g., 0.02 K/yr and 0.02 g/kg/yr in Zika et al., 2018).

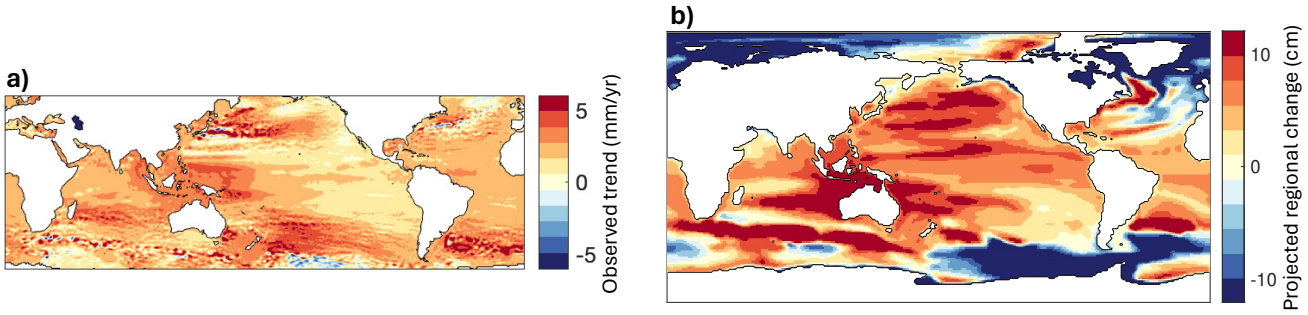

Figure S1. Maps of observed and projected regional sea level changes. (a) Observed sea level trends during 1993 to 2018, computed using the AVISO satellite altimetry dataset (Ducet et al., 2000). Only the latitude range 60°S–60°N is plotted due to limited data coverage in higher latitudes. (b) Projected future regional pattern of sea level change generated using the GFDL-ESM2M simulation of the CMIP5 scenario RCP 4.5, shown as the average during years 2090-2099 compared with 2006-2015. The simulation results include dynamic contributions due to changes in ocean density and mass redistribution, as well as land ice and terrestrial water components which are calculated using a separate modeling framework (for details see main text as well as Church et al., 2013). Here the global-mean sea level rise, which is 41 cm, is subtracted from the future projection in order to better illustrate the regional patterns.

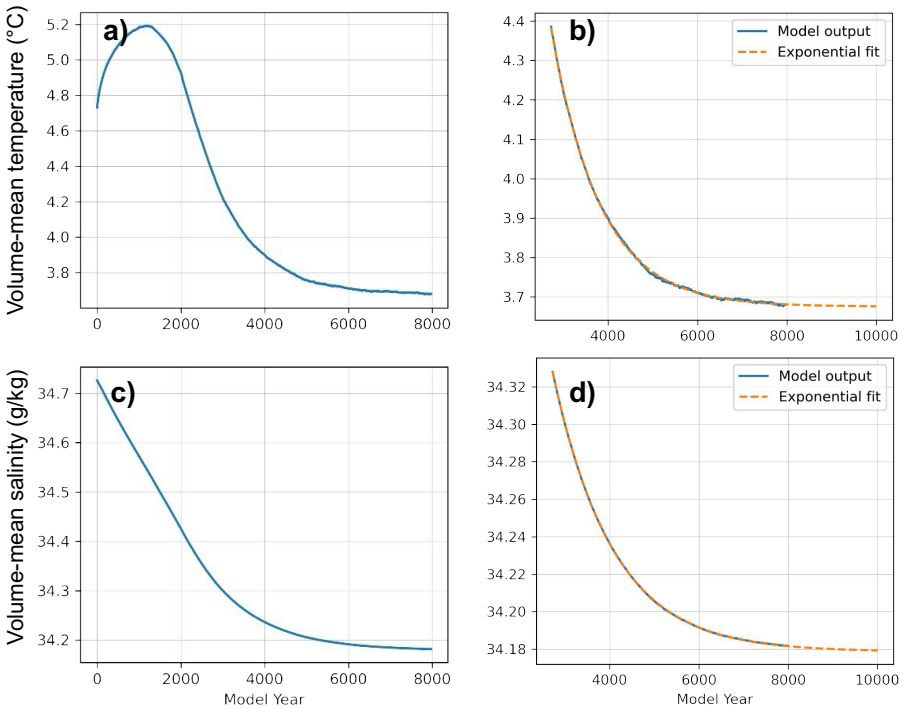

Figure S2. Evolution of (a,b) temperature and (c,d) salinity during (a,c) the entire Spin-up simulation and (b,d) the final 5000 years of the 7975-year Spin-up simulation. The dashed lines show exponential fits, with e-folding timescales of 1090 years for temperature and 1340 years for salinity.

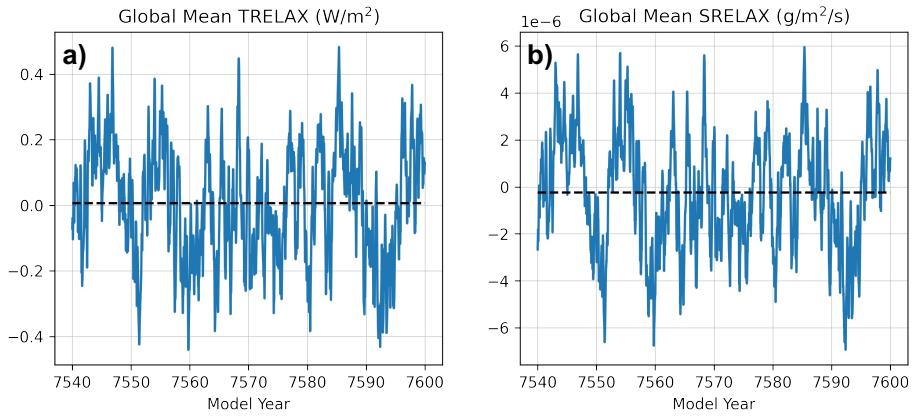

Figure S3. Evolution of the global-mean value of (a) the heat flux and (b) the salt flux due to the surface relaxation conditions during years 7540-7599 of the Spin-up simulation. The black dashed line shows the time average. The fluxes during the time period plotted here are used as the fixed surface fluxes in the Control, Surface, and Deep simulations.

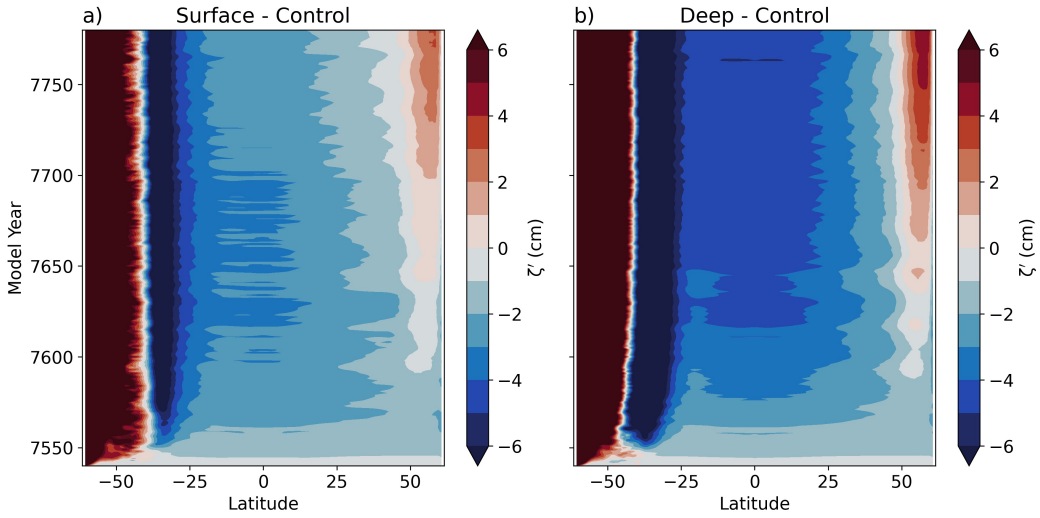

Figure S4. Hovmöller plots showing the zonal-mean dynamic sea level anomaly ζ' as a function of latitude and time in (a) the Surface simulation and (b) the Deep simulation.

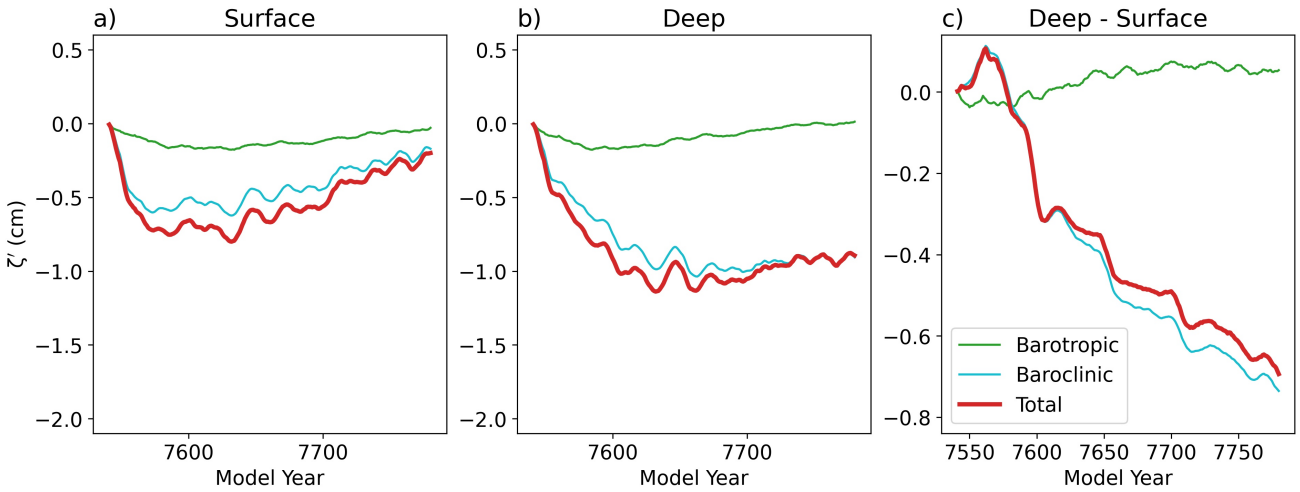

Figure S5. As in Fig. 4, but using a decomposition of Northern Hemisphere dynamic sea level anomaly ζ' into components associated with barotropic and baroclinic circulation changes (McWilliams et al., 2024), rather than components associated with mass redistribution and steric changes (Gill & Niiler, 1973; Yin et al., 2010; Griffies et al., 2014; Gregory et al., 2019). Here, only the sea level away from the continental shelves is decomposed, as per the requirements in McWilliams et al. (2024).

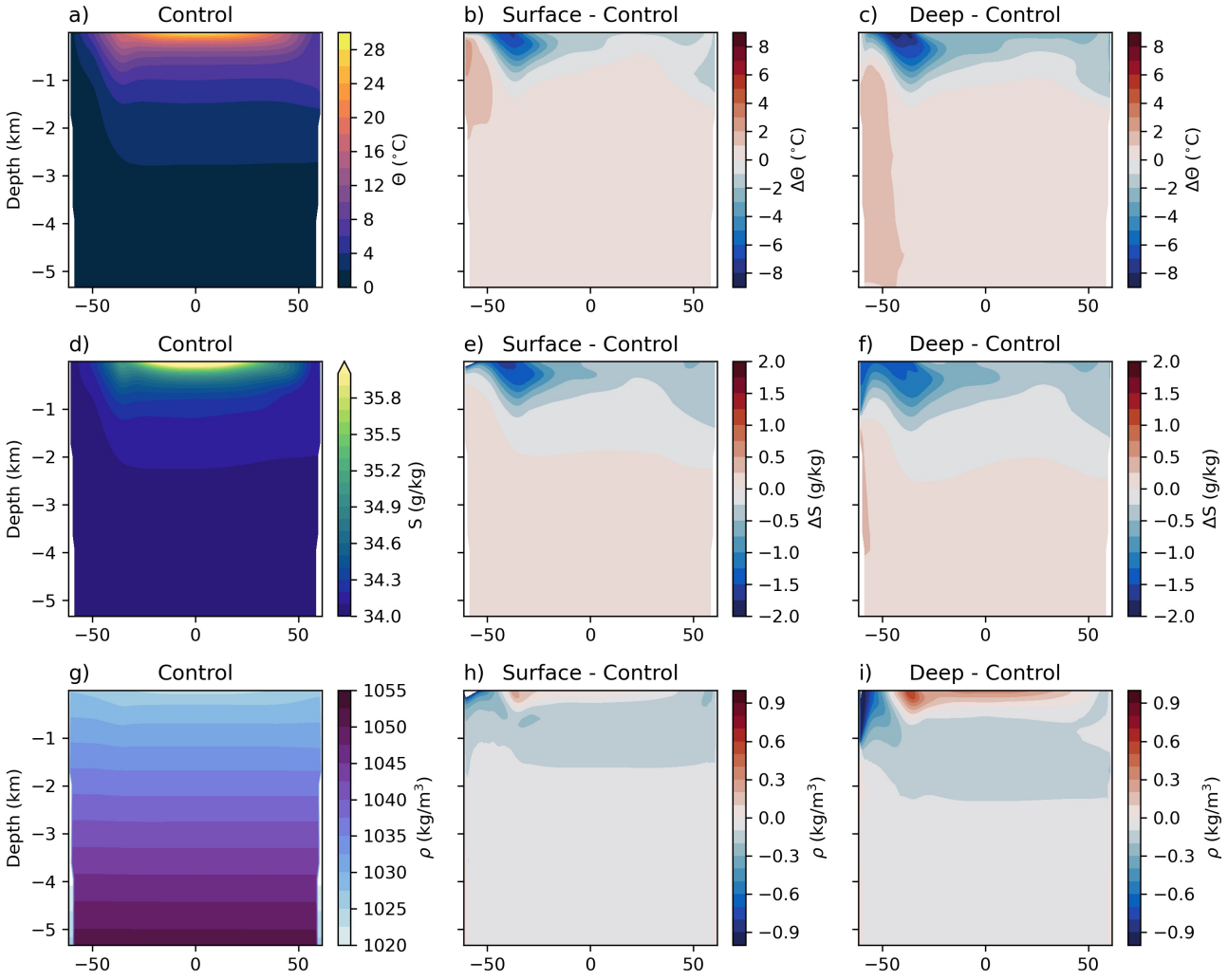

Figure S6. Zonal-mean cross sections of potential temperature θ (top), salinity S (middle), and density ρ (bottom), averaged over the final decade of each simulation.

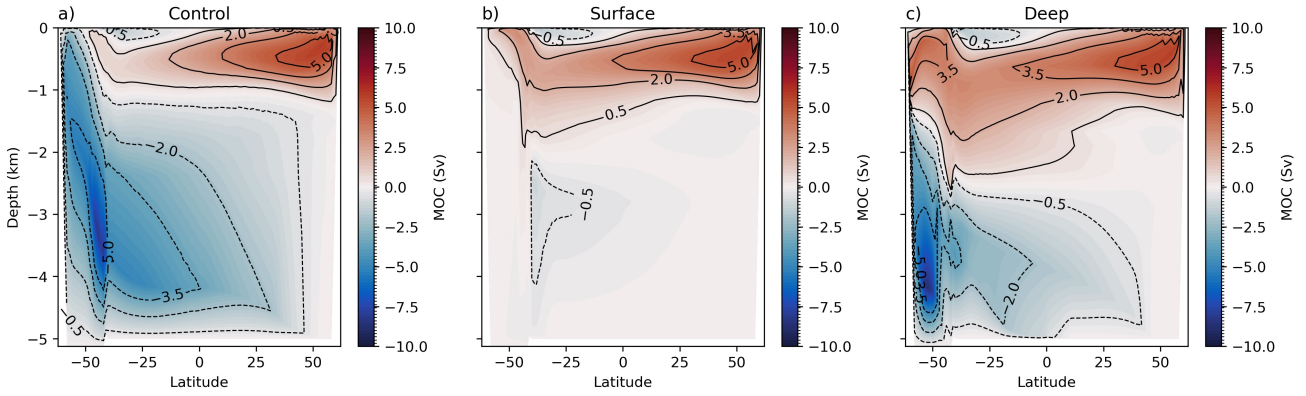

Figure S7. Meridional overturning circulation streamfunction in each simulation. The time-mean residual streamfunction during the final decade of each simulation is calculated in potential density coordinates utilizing the MITgcm layers package. The streamfunction then is remapped to depth coordinates using the depth of each potential density surface averaged zonally and over the final decade of each simulation. Positive values (represented with solid lines and red color) indicate a clockwise circulation.

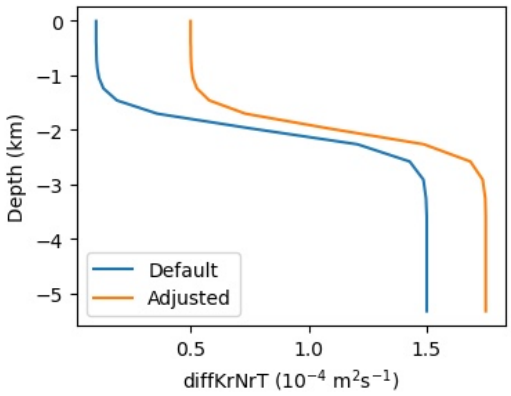

Figure S8. The default profile used during the sensitivity testing (blue) and the adjusted profile used in the simulations presented here (orange) for the background vertical diffusivity of temperature ("diffKrNrT") and equivalently salinity ("diffKrNrS"). This is specified in MITgcm as a parameter value at each vertical level.

References

Church, J., Clark, P., Cazenave, A., Gregory, J., Jevrejeva, S., Levermann, A., ... Unnikrishnan, A. (2013). Chapter 13, Sea level change. In T. Stocker et al. (Eds.), *Climate Change 2013: The Physical Science Basis. Contribution of Working Group I to the Fifth Assessment Report of the Intergovernmental Panel on Climate Change.* Cambridge University Press, Cambridge, UK.

Ducet, N., Traon, P. Y. L., & Reverdin, G. (2000). Global high-resolution mapping of ocean circulation from TOPEX/Poseidon and ERS-1 and -2. *J. Geophys. Res.*, *105*(C8), 19477–19498. ((AVISO Ssalto/Duacs monthly data accessed from https://www.aviso.altimetry.fr/en/data/data-access.html)) doi: 10.1029/2000JC900063

Gill, A. E., & Niiler, P. P. (1973). Theory of seasonal variability in ocean. *Deep-sea Res.*, *20*(2), 141–177. doi: 10.1016/0011-7471(73)90049-1

Gregory, J., Griffies, S., Hughes, C., Lowe, J., Church, J., Fukimori, I., ... van de Wal, R. (2019). Concepts and terminology for sea level: Mean, variability and change, both local and global. *Surv. Geophys.*, 1–39. doi: 10.1007/s10712-019-09525-z

Griffies, S. M., Yin, J. J., Durack, P. J., Goddard, P., Bates, S. C., Behrens, E., ... Zhang, X. B. (2014). An assessment of global and regional sea level for years 1993-2007 in a suite of interannual CORE-II simulations. *Ocean Modelling*, *78*, 35–89. doi: 10.1016/j.ocemod.2014.03.004

Killworth, P. D. (1996). Time interpolation of forcing fields in ocean models. *J. Phys. Oceanogr.*, *26*(1), 136–143. doi: 10.1175/1520-0485(1996)026¡0136:TIOFFI¿2.0.CO;2

McWilliams, J. C., Molemaker, M. J., & Damien, P. (2024). Baroclinic sea level. *J. Adv. In Modeling Earth Systems*, *16*(4), e2023MS003977. doi: 10.1029/2023MS003977

Yin, J. J., Griffies, S. M., & Stouffer, R. J. (2010). Spatial variability of sea level rise in twenty-first century projections. *J. Climate*, *23*(17), 4585–4607. doi: 10.1175/2010JCLI3533.1

Zika, J. D., Skliris, N., Blaker, A. T., Marsh, R., Nurser, A. J. G., & Josey, S. A. (2018). Improved estimates of water cycle change from ocean salinity: the key role of ocean warming. *Environmental Res. Lett.*, *13*(7), 074036. doi: 10.1088/1748-9326/aace42